

How to Avoid Artificial Boundaries in the Numerical Calculation of Black Hole Spacetimes

Peter Hübner

(pth@aei-potsdam.mpg.de)

Max-Planck-Institut für Gravitationsphysik
Albert-Einstein-Institut
Schlaatzweg 1
D-14473 Potsdam
FRG

short title: Calculating Black Hole Spacetimes

PACS numbers: 0420G, 0420H, 0430

This is the first of a series of papers describing a numerical implementation of the conformally rescaled Einstein equation, an implementation designed to calculate asymptotically flat spacetimes, especially spacetimes containing black holes.

In the present paper we derive the new first order time evolution equations to be used in the scheme. These time evolution equations can either be written in symmetric hyperbolic or in flux-conservative form. Since the conformally rescaled Einstein equation, also called the conformal field equations, formally allow us to place the grid boundaries outside the physical spacetime, we can modify the equations near the grid boundaries and get a consistent and stable discretisation. Even if we calculate spacetimes containing black holes, there is no need for introducing artificial boundaries in the physical spacetime, which then would complicate, influence, or even exclude the computation of certain spacetime regions.

I. INTRODUCTION

Since the capacity of computers has been rapidly growing over the last years, numerical experiments on spacetimes without symmetries are now in the reach of the available hardware resources. Numerical relativity is on the way to take the step which has already been taken in other fields of physics: Numerical experiments supplement, or sometimes even replace, real experiments.

When designing the computer programs for the numerical experiments it is highly important to be aware of the following significant difference to other fields of physics: One of the major methods in developing codes for numerical experiments has been the comparison and testing with real experiments. In numerical relativity however, such possibilities are very rare and limited; appropriate experiments are not available, comparison with observations of astrophysical events requires the knowledge of many unknown parameters, and the known exact solutions presumably do not represent the full spectrum of properties of solutions of the non-linear Einstein equation.

The author, therefore, believes, that reliability of the results of numerical experiments in

relativity can only be ensured by mathematical rigor of the implemented algorithms, i. e. their vanishing grid size limit should be consistent with the Einstein equation.

In this series of papers we describe a numerical implementation of the conformal field equations [1,2]. In this implementation we do not use any approximation besides the idealisation of isolated systems and the replacement of the partial differential equations by their discretised versions. The approach described below is designed to be able to calculate global as well as local properties of spacetimes arising from data of arbitrary strength. Important issues are e. g. testing the validity range of approximations, calculating the long-time behaviour of fields, and investigating the nature of singularities. For spherically symmetric models with scalar fields the attainability of these goals has been demonstrated in [3,4].

The approach described is so powerful that we can use the same time evolution scheme to calculate scenarios like the decay of weak gravitational waves to Minkowski space or the merging of black holes.

The use of the conformal field equations allows us to extend the calculation to null infinity. Moreover, we can formally even extend the spacetime through null infinity and place the grid boundaries in a region which is causally disconnected from the physical spacetime. Then boundary effects, like a violation of the constraints or creation of spurious backscattering, cannot propagate into the physical spacetime. As null infinity is part of the grid, we can calculate anything which is suggested by a Penrose diagram, including quantities which are only defined in the limit of going to infinity, like gravitational radiation.

Since an exhaustive description of the new ingredients needed for this $(n+1)$ -dimensional ($n \leq 3$) implementation of the conformal approach is too long for a single paper and requires techniques from mathematical relativity as well as numerical mathematics, we have split it into a series of papers. In this first part of the series we describe the foundation of the time evolution part of the code, namely the geometrical background, the equations used, and the physical scenarios which will be treated in detail in the following articles. In particular, we develop the mathematical basis and give a preview over the result which can be expected from our numerical approach.

Details about the initial data problem, the discretisation used, the tests, and more will be found in the following parts of the series.

In section II the conformal field equations are written in first order form and split into symmetric hyperbolic time evolution equations and constraints. When deriving this new form, which could also be written in flux conservative form, we proceed in analogy to [5], a paper dealing with the Einstein equations for vacuum in physical spacetime. Also, these properties of the conformal field equations are recalled which are essential for the following. Having the conventions available we discuss the hyperboloidal initial value problem in section III. There we also explain the special role of the conformal factor, special not as a variable of the system, but special when the physical spacetime is reconstructed from the variables of the conformal field equation. Section IV describes possible grid boundary treatments and proves their numerical stability.

In the last section we outline the power of the conformal approach by describing why we can in principle calculate the complete future evolution of the initial data, including null infinity. Since conformal rescaling preserves the null cone structure of a spacetime, the conformal approach is especially tuned for analysing causal structure and gravitational radiation.

II. A SYMMETRIC HYPERBOLIC FIRST ORDER SYSTEM FOR THE CONFORMAL FIELD EQUATIONS

We start the derivation of the first order equations by giving the conformal field equations in our notation and recalling some of their properties, whose proofs can be found in [6,3].

A. The conformal field equations and the reconstruction of physical spacetime

In the conformal approach we solve the initial value problem for the conformal field equations, which read

$$\nabla_a \hat{R}_{bc} - \nabla_b \hat{R}_{ac} + \frac{1}{12} ((\nabla_a R) g_{bc} - (\nabla_b R) g_{ac}) + 2 (\nabla_d \Omega) d_{abc}{}^d = 0, \quad (1a)$$

$$\nabla_d d_{abc}{}^d = 0, \quad (1b)$$

$$\nabla_a \nabla_b \Omega_a + \frac{1}{2} \hat{R}_{ab} \Omega - \frac{1}{4} \nabla^a \nabla_a \Omega g_{ab} = 0, \quad (1c)$$

$$\frac{1}{4} \nabla_a (\nabla^b \nabla_b \Omega) + \frac{1}{2} \hat{R}_{ab} \nabla^b \Omega + \frac{1}{24} \Omega \nabla_a R + \frac{1}{12} \nabla_a \Omega R = 0, \quad (1d)$$

$$\Omega d_{abc}{}^d + (g_{ca} \hat{R}_b{}^d - g_{cb} \hat{R}_a{}^d - g^d{}_a \hat{R}_{bc} + g^d{}_b \hat{R}_{ac})/2 + (g_{ca} g_b{}^d - g_{cb} g_a{}^d) \frac{R}{12} = R_{abc}{}^d, \quad (1e)$$

and

$$\Omega^2 R + 6 \Omega \nabla^a \nabla_a \Omega - 12 (\nabla^a \Omega) (\nabla_a \Omega) = 0. \quad (1f)$$

Here the tensor g_{ab} is a Lorentzian metric on a manifold M , \hat{R}_{ab} a symmetric-traceless tensor field, $d_{abc}{}^d$ a tensor field with the symmetries of the Weyl tensor, Ω a scalar, $R_{abc}{}^d$ the differential expression of the Riemann tensor in terms of the metric g_{ab} , R a prescribed function on M , and ∇_a denotes the derivative operator associated to g_{ab} .

For any solution $(g_{ab}, \hat{R}_{ab}, d_{abc}{}^d, \Omega)$ of system (1) the function R turns out to be the Ricci scalar, \hat{R}_{ab} the traceless part of the Ricci tensor, and $\Omega d_{abc}{}^d$ the Weyl tensor of g_{ab} .

Any solution of (1a–1d) solves (1f) on a connected domain if (1f) holds at one point in the domain. It is, therefore, sufficient to enforce (1f) as a constraint on the initial data. In the following this requirement will no longer be explicitly mentioned.

We will arrange our calculation such that (M, g_{ab}) will be a globally hyperbolic manifold sliced by the spacelike hypersurfaces Σ_t . By solving (1) on M we obtain a solution of the Einstein equation on the physical spacetime $\tilde{M} := \{x \in M \mid \Omega(x) > 0\}$, since for any sufficiently smooth solution of (1a–1d) the metric $\tilde{g}_{ab} := \Omega^{-2} g_{ab}$ is a solution of the Einstein equation on \tilde{M} .

It is sufficient for our purposes to only consider setups for which the physical part $\tilde{\Sigma}_{t_0} := \{x \in \Sigma_{t_0} \mid \Omega(x) > 0\}$ of the initial hypersurface Σ_{t_0} is relatively compact. We define $\mathcal{S}_t := \{x \in \Sigma_t \mid \Omega(x) = 0\}$.

The part of the boundary of \tilde{M} with $\nabla_a \Omega|_{\Omega=0} \neq 0$ is denoted \mathcal{J} . All geodesics of \tilde{g}_{ab} which end at \mathcal{J} are null geodesics. Since they intersect \mathcal{J} at infinite affine parameter with respect to \tilde{g}_{ab} , \mathcal{J} is infinitely far away with respect to \tilde{g}_{ab} . \mathcal{J} represents, therefore, null infinity, and quantities like gravitational radiation, which is extracted most effectively by taking the limit of going to infinity, can be determined by reading off the values of certain variables at \mathcal{J} .

As can be seen immediately from equation (1f), \mathcal{J} is a null hypersurface. When solving the initial value problem for data given on the spacelike hypersurface Σ_{t_0} , we will, unless mentioned otherwise, require $\nabla^a \Omega$ to be future directed everywhere on $\mathcal{S} := \{P \in \Sigma_{t_0} \mid \Omega(P) = 0\}$. Or stated more interpretatively, we choose the initial hypersurface in such a way that it intersects future null infinity and not past null infinity. Then $\tilde{\Sigma}_{t_0} := \tilde{M} \cap \Sigma_{t_0}$ is a Cauchy surface for the part of \tilde{M} which lies in the future of Σ_{t_0} , i. e. $\tilde{M} \cap \mathcal{D}(\Sigma_{t_0}) = \mathcal{D}(\tilde{M} \cap \Sigma_{t_0})$, where \mathcal{D} denotes the future domain of dependence.¹ This property guarantees that at the points of $\{x \mid \Omega(x) \geq 0\}$ the solution of the initial value problem is independent of the values of the variables at the points in $\{x \mid \Omega(x) < 0\}$. Hence, by placing the grid boundaries outside physical spacetime, namely into the set $\{x \mid \Omega(x) < 0\}$, we gain a decoupling of the boundary treatment from the calculation of physical spacetime.

If $\mathcal{J} = R \times \mathcal{S}$ consists of (disconnected) pieces with topology $R \times S^2$, the spacetime is called (weakly) asymptotically flat [8]. The gravitational wave scenarios usually treated fall into this class. The conformal field equations also allow us to study data with other topologies of \mathcal{S} , and in fact many aspects of gravitational radiation can also be studied on such spacetimes. We will see in subsection III B 2, that in numerical studies spacetimes with toroidal sections of \mathcal{J} may provide advantages over those with $\mathcal{J} = R \times S^2$, especially in the cases where we reduce the space dimensions by assuming symmetries. To have a term available which refers to both cases we call spacetimes **asymptotically regular**,² if they arise from regular data for the conformal field equations with $\nabla_a \Omega$ future directed everywhere on \mathcal{S}_{t_0} . The conformal and the physical metric are related by a rescaling which is essentially arbitrary, as two solutions (M, g_{ab}, Ω) and $(M, \bar{g}_{ab}, \bar{\Omega})$ with $(\bar{g}_{ab}, \bar{\Omega}) = (\theta^2 g_{ab}, \theta \Omega)$ and a positive function θ describe the same physical spacetime. Under the rescaling θ the Ricci scalar R changes. To obtain equations with nice properties we do not prescribe Ω but R . The prescribed function R is therefore a gauge source function for the rescaling gauge.

The equations (1a), (1b) and (1d) are third order equations for the metric g_{ab} and the conformal factor Ω . To be able to apply standard theorems which imply well-posedness of the initial value problem, we introduce appropriate gauge conditions and formulate the equations (1) as a symmetric hyperbolic first order system. There are various possibilities to do this. In all variants gauge source functions must be specified to make the solution of the initial value problem unique. In the variants which use the spinor [6,7] or the frame formalism [9,10] the coordinate gauge freedom is fixed by 10 gauge source functions (4 degrees of freedom for the coordinates, 6 for the tetrad). In the variant to be described here, which uses a 3-tensor formalism, the coordinate gauge freedom is fixed by the three components of the shift vector and a function which is closely related to the lapse function.

The possible implementations of the conformal field equations differ slightly in the number of variables, the gauge conditions, and the type of non-linearity. Our propagation equations allow us to write them in flux conservativ form. Whether one of the implementations has significant advantages over the others in numerical calculations remains to be seen. A nu-

¹ $\mathcal{D}(S) := \{P \in M \mid \text{Every past inextendible causal curve through } P \text{ intersects } S\}$

²regular with respect to the existence of null infinity, the spacetime may nevertheless contain singularities.

merical comparison with [7,11] is planned (see also subsection III B 2).

Many quantities of physical interest, like gravitational radiation or tidal forces (geodesic deviation), can be expressed in terms of the components of the conformal Weyl tensor $d_{abc}{}^d$ or the physical Riemann tensor. As the systems just mentioned contain the components of the conformal curvature as variables, those quantities can be calculated by pure algebra and their error can be estimated by a convergence analysis.

B. The 3+1 split of the conformal field equations

1. Equations for the lower order quantities

Proceeding in analogy to [5] we introduce the extrinsic curvature k_{ab} as new variable. It is related to the 3-metric³ h_{ab} and the hypersurface normal³ n^a by the equation

$$\mathcal{L}_n h_{ab} - 2k_{ab} = 0. \quad (2a)$$

The connection $\Gamma^a{}_{bc}$ relates to the curvature $R_{abc}{}^d$ by

$$-\partial_a \Gamma^d{}_{bc} + \partial_b \Gamma^d{}_{ac} + \Gamma^e{}_{ca} \Gamma^d{}_{be} - \Gamma^e{}_{cb} \Gamma^d{}_{ae} - R_{abc}{}^d = 0. \quad (2b)$$

Equation (1c) and (1d), the equations for the conformal factor Ω , are written in first order form as follows,

$$\nabla_a \Omega - {}^{(4)}\Omega_a = 0, \quad (2c)$$

$$\nabla_a {}^{(4)}\Omega_b + \frac{1}{2} \hat{R}_{ab} \Omega - \omega g_{ab} = 0, \quad (2d)$$

with $\omega = \frac{1}{4} \nabla^a \nabla_a \Omega$, and

$$\nabla_a \omega + \frac{1}{2} \hat{R}_{ab} {}^{(4)}\Omega^b + \frac{1}{24} \Omega \nabla_a R + \frac{1}{12} {}^{(4)}\Omega_a R = 0. \quad (2e)$$

In the equation for the tracefree Ricci tensor \hat{R}_{ab} we substitute the derivatives of Ω ,

$$\nabla_{[a} \hat{R}_{b]c} + \frac{1}{12} (\nabla_{[a} R) g_{b]c} + {}^{(4)}\Omega_d d_{abc}{}^d = 0. \quad (2f)$$

The equation for the conformal Weyl tensor $d_{abc}{}^d$,

$$\nabla_d d_{abc}{}^d = 0, \quad (2g)$$

is kept.

We now make a 3+1 split of the system (2) by a straightforward extension of the treatment given in [5]. For completeness the essential definitions are repeated but for further clarification the reader is advised to consult this reference.

The globally hyperbolic manifold (M, g_{ab}) is sliced with spacelike hypersurfaces Σ_t . The

³definition follows

parameter t then provides a natural time coordinate and we can introduce a timelike vector field t^a related to t by $t^a \nabla_a t = 1$. Denoting the unit normal of the hypersurface Σ_t by n^a , n^a and t^a are related by

$$n^a = \frac{1}{N}(t^a - N^a), \quad (3)$$

with N the lapse function and N^a the shift vector. The metric g_{ab} induces a 3-metric h_{ab} on each Σ_t by

$$g_{ab} = h_{ab} - n_a n_b. \quad (4)$$

We define

$$a_a := n^b \nabla_b n_a. \quad (5)$$

The object $a_a = \frac{h_a^b \partial_b N}{N}$ is purely spatial.⁴ Later the coordinate gauge freedom is fixed by specifying the three components of the shift vector N^a and the function $q := \ln(\frac{N}{\sqrt{h}})$ as free functions of space and time. The following holds:

$$a_a = h_a^b \partial_b q + \gamma_{ab}^b. \quad (6)$$

γ_{bc}^a is the 3-connection for the 3-metric h_{ab} and is used as a variable of the first order system. The 4-connection Γ_{bc}^a is decomposed into 3-parts by means of the hypersurface normal,

$$\begin{aligned} \Gamma_{bc}^a = & \text{}^{(1,1,1)}\Gamma_{bc}^a - n^a \text{}^{(0,1,1)}\Gamma_{bc} - \text{}^{(1,0,1)}\Gamma_c^a n_b - \text{}^{(1,0,1)}\Gamma_b^a n_c \\ & + \text{}^{(1,0,0)}\Gamma^a n_b n_c + n^a \text{}^{(0,0,1)}\Gamma_b n_c + n^a \text{}^{(0,0,1)}\Gamma_c n_b - n^a \text{}^{(0,0,0)}\Gamma n_b n_c, \end{aligned} \quad (7)$$

where a $(\dots, 0, \dots)$ in front of a quantity indicates contraction with n^a and a $(\dots, 1, \dots)$ means projected with h_a^b , e.g. $\text{}^{(1,0,1)}\Gamma_c^a := h_a^d n^b h_c^e \Gamma_{be}^d$. A calculation shows

$$\text{}^{(0,0,0)}\Gamma = -\frac{n^a \partial_a N}{N} \quad (8a)$$

$$\text{}^{(1,0,0)}\Gamma^a = \frac{n^b \partial_b N^a}{N} + a^a \quad (8b)$$

$$\text{}^{(0,0,1)}\Gamma_b = -a_b \quad (8c)$$

$$\text{}^{(0,1,1)}\Gamma_{bc} = -k_{bc} \quad (8d)$$

$$\text{}^{(1,0,1)}\Gamma_b^a = k_b^a + \frac{1}{N} h_b^c \partial_c N^a \quad (8e)$$

$$\text{}^{(1,1,1)}\Gamma_{bc}^a = \gamma_{bc}^a \quad (8f)$$

For the decomposition of the curvature variables we get

$$\hat{R}_{ab} = \text{}^{(1,1)}\hat{R}_{ab} - n_a \text{}^{(0,1)}\hat{R}_b - \text{}^{(0,1)}\hat{R}_a n_b + n_a n_b \text{}^{(0,0)}\hat{R} \quad (9)$$

and

⁴can be calculated on Σ_t by only knowing the values of N , N^a , and h_a^b on Σ_t

$$d_{abcd} = l_{db}E_{ac} - l_{da}E_{bc} - l_{cb}E_{ab} + l_{ca}E_{bd} \\ - n_b B_{ae} {}^{(3)}\epsilon^e{}_{dc} + n_a B_{bf} {}^{(3)}\epsilon^e{}_{dc} - n_d B_{cf} {}^{(3)}\epsilon^e{}_{ba} + n_c B_{df} {}^{(3)}\epsilon^e{}_{ba}, \quad (10)$$

with $l_{ab} = h_{ab} + n_a n_b$, ${}^{(3)}\epsilon_{bcd} = n^a \epsilon_{abcd}$, $E_a{}^a = 0$, and $B_a{}^a = 0$. As \hat{R}_{ab} is tracefree, ${}^{(0,0)}\hat{R} = {}^{(1,1)}\hat{R}_a{}^a$.

For the derivatives of Ω we substitute

$$\Omega_0 := n^a \nabla_a \Omega = n^a {}^{(4)}\Omega_a \quad (11)$$

and

$$\Omega_a := h_a{}^b \nabla_b \Omega = h_a{}^b {}^{(4)}\Omega_b. \quad (12)$$

The set of 3-variables is now complete, it is $(h_{ab}, k_{ab}, \gamma^a{}_{bc}, {}^{(0,1)}\hat{R}_a, {}^{(1,1)}\hat{R}_{ab}, E_{ab}, B_{ab}, \Omega, \Omega_0, \Omega_a, \omega)$.

2. The split into time evolution equations and constraints

Contracting all indices of the equations (2) with n^a respectively $h_a{}^b$ and using the new variables we obtain time evolution equations (equations with ∂_t) and constraints (equations without ∂_t). Although this calculation is lengthy, it is straightforward. To perform it the author has used a MATHTECTOR program for doing 3+1 decompositions written by himself. Then, after removing the gauge freedom by fixing gauge source functions and adding constraints to the time evolution equations to achieve symmetric hyperbolicity, we obtain a complete set of symmetric hyperbolic time evolution equations. We write the equations in terms of the null quantities \mathcal{N} , the corresponding equations are obtained by setting the null quantities to 0:

$$\mathcal{N}_{\mathbf{h}ab} = -\mathcal{L}_n h_{ab} + 2k_{ab} \quad (13a)$$

$$\mathcal{N}_{\mathbf{k}ab} = -\mathcal{L}_n k_{ab} + {}^{(3)}\nabla_c \gamma^c{}_{ab} + \gamma^d{}_{bc} \gamma^c{}_{ad} + a_a a_b + k_c{}^c k_{ab} - \gamma^c{}_{ab} a_c \\ + h_a{}^c h_b{}^d \partial_d \partial_c q - \frac{R}{12} h_{ab} - {}^{(1,1)}\hat{R}_c{}^c h_{ab} - 2\Omega E_{ab} \quad (13b)$$

$$\mathcal{N}_{\gamma^a{}_{bc}} = -h_{ad} \mathcal{L}_n \gamma^d{}_{bc} + {}^{(3)}\nabla_a k_{bc} - a_a k_{bc} + a_c k_{ab} + a_b k_{ac} + h_{da} h_b{}^e h_c{}^f \frac{1}{N} \partial_f \partial_e N^d \\ - \frac{1}{2} h_{ac} {}^{(0,1)}\hat{R}_b - \frac{1}{2} h_{ab} {}^{(0,1)}\hat{R}_c + h_{bc} {}^{(0,1)}\hat{R}_a + {}^{(3)}\epsilon_{ac}{}^d \Omega B_{db} + {}^{(3)}\epsilon_{ab}{}^d \Omega B_{dc} \quad (13c)$$

$$\mathcal{N}_{\mathbf{E}ab} = -\mathcal{L}_n E_{ab} + \frac{1}{2} {}^{(3)}\epsilon_a{}^{cd} {}^{(3)}\nabla_d B_{cb} + \frac{1}{2} {}^{(3)}\epsilon_b{}^{cd} {}^{(3)}\nabla_d B_{ca} + a^c {}^{(3)}\epsilon_{cb}{}^d B_{da} + a^c {}^{(3)}\epsilon_{ca}{}^d B_{db} \\ - h_{ab} k^{cd} E_{cd} + \frac{5}{2} k_b{}^c E_{ca} + \frac{5}{2} k_a{}^c E_{cb} - 2k_c{}^c E_{ab} \quad (13d)$$

$$\mathcal{N}_{\mathbf{B}ab} = -\mathcal{L}_n B_{ab} - \frac{1}{2} {}^{(3)}\epsilon_a{}^{cd} {}^{(3)}\nabla_d E_{cb} - \frac{1}{2} {}^{(3)}\epsilon_b{}^{cd} {}^{(3)}\nabla_d E_{ca} + a^c {}^{(3)}\epsilon_{bc}{}^d E_{da} + a^c {}^{(3)}\epsilon_{ac}{}^d E_{db} \\ - h_{ab} k^{cd} B_{cd} + \frac{5}{2} k_b{}^c B_{ca} + \frac{5}{2} k_a{}^c B_{cb} - 2k_c{}^c B_{ab} \quad (13e)$$

$$\mathcal{N}_{(0,1)\hat{\mathbf{R}}a} = -\mathcal{L}_n {}^{(0,1)}\hat{R}_a + {}^{(3)}\nabla_b {}^{(1,1)}\hat{R}_a{}^b - \frac{1}{4} {}^{(3)}\nabla_a R - k_b{}^b {}^{(0,1)}\hat{R}_a + a_b {}^{(1,1)}\hat{R}_a{}^b + a_a {}^{(1,1)}\hat{R}_b{}^b \quad (13f)$$

$$\mathcal{N}_{(1,1)\hat{\mathbf{R}}ab} = -h_{bc} \mathcal{L}_n {}^{(1,1)}\hat{R}_a{}^c + {}^{(3)}\nabla_a {}^{(0,1)}\hat{R}_b - \frac{1}{12} h_{ab} \mathcal{L}_n R + a_b {}^{(0,1)}\hat{R}_a + a_a {}^{(0,1)}\hat{R}_b$$

$$-k_{ab}^{(1,1)}\hat{R}_c^c - k_{cb}^{(1,1)}\hat{R}_a^c - 2^{(3)}\epsilon^{cd}_b\Omega_c B_{da} - 2\Omega_0 E_{ab} \quad (13g)$$

$$\mathcal{N}_\Omega = -\mathcal{L}_n\Omega + \Omega_0 \quad (13h)$$

$$\mathcal{N}_{\Omega_0} = -\mathcal{L}_n\Omega_0 - \omega + a^a\Omega_a - \frac{\Omega}{2}^{(1,1)}\hat{R}_a^a \quad (13i)$$

$$\mathcal{N}_{\Omega_a} = -\mathcal{L}_n\Omega_a + a_a\Omega_0 + k_a^b\Omega_b - \frac{\Omega}{2}^{(0,1)}\hat{R}_a \quad (13j)$$

$$\mathcal{N}_\omega = -\mathcal{L}_n\omega - \frac{\Omega}{24}\mathcal{L}_nR - \frac{R}{12}\Omega_0 - \frac{\Omega^a}{2}^{(0,1)}\hat{R}_a + \frac{\Omega_0}{2}^{(1,1)}\hat{R}_a^a \quad (13k)$$

Note that for a 3-tensor $t_{...a...}^{...b...}$ the following equality holds:

$$\mathcal{L}_n t_{...a...}^{...b...} = \frac{1}{N} (\mathcal{L}_t - \mathcal{L}_N) t_{...a...}^{...b...} + \dots + n^b t_{...a...}^{...c...} a_c + \dots$$

The operator $^{(3)}\nabla_a$ is the covariant derivative preserving the 3-metric h_{ab} . If one uses new variables for E_{ab} and B_{ab} as in [5], this system is indeed symmetric hyperbolic. The equations (13a–13e) have the same principal part as the corresponding equations (6.4–6.8) in [5]. The principal parts of (13a) and (13h–13k) are equal, the same is true for the principal parts of the subsystems (13b,13c) and (13f,13g). Therefore the system (13) possesses the same characteristics as the equations (6.4–6.8) in [5], namely they are either null hypersurfaces with respect to g_{ab} or they are timelike and tangent to n^a or to the timelike cone $\{c_{ab}t^at^b = 0\}$ where $c_{ab} = 4h_{ab} - n_an_b$. Since all characteristics are within the light cone of g_{ab} , the system is consistent with Einstein causality.

The treatment of the coordinate gauge freedom (fixed by the functions q and N^a) is also discussed in more detail in [5]. What is said there extends straightforwardly to the rescaling freedom fixed by the gauge source function R .

For the numerical treatment the equation (13c) is multiplied by h^{ea} and the h_{bc} in (13g) is moved into the Lie derivative. Both manipulations are done to get $\frac{1}{N}$ times the identity matrix in front of the time derivative and the second is also done to obtain the 6 components of the symmetric tensor $^{(1,1)}\hat{R}_{ab}$ instead of the 9 components of $^{(1,1)}\hat{R}_a^b$ as variables of the system. The two equations resulting from $\mathcal{N}_{(1,1)\hat{\mathbf{R}}_{ab}}$ and $\mathcal{N}_{(1,1)\hat{\mathbf{R}}_{ba}}$ are identical only up to constraints and we take the arithmetic mean of the two null quantities. By this averaging some characteristics change but they remain within the light cone of g_{ab} .

The system (13) can also be written in flux conservative form. The results we obtained by solving the flux conservative system with a rotated Richtmyer scheme were less accurate than those obtained by solving the quasilinear form (13) with the same scheme. Furthermore calculations on a simple non-linear model system showed that damping of grid modes is weaker for the flux-conservative form. Therefore, the quasilinear form of the equations seems to be better suited for our application than the flux conservative form and we refrain from presenting the flux conservative form of the system.

The null quantities not appearing in the system (13) are the constraints:

$$\mathcal{N}_{\mathbf{h}abc} = ^{(3)}\nabla_a h_{bc} \quad (14a)$$

$$\mathcal{N}_{\mathbf{k}abc} = -^{(3)}\nabla_a k_{bc} + ^{(3)}\nabla_b k_{ac} + \frac{1}{2}h_{ca}^{(0,1)}\hat{R}_b - \frac{1}{2}h_{cb}^{(0,1)}\hat{R}_a - ^{(3)}\epsilon_{ab}^d \Omega B_{dc} \quad (14b)$$

$$\mathcal{N}_{\gamma abc}^d = -^{(3)}\nabla_a \gamma_{bc}^d + ^{(3)}\nabla_b \gamma_{ac}^d + \gamma_{ae}^d \gamma_{bc}^e - \gamma_{be}^d \gamma_{ac}^e$$

$$\begin{aligned}
& -k_a^d k_{bc} + k_{ac} k_b^d + \frac{1}{12} h_a^d h_{bc} R - \frac{1}{12} h_{ac} h_b^d R \\
& - \frac{1}{2} h_b^d {}^{(1,1)}\hat{R}_{ac} + \frac{1}{2} h_a^d {}^{(1,1)}\hat{R}_{bc} - \frac{1}{2} h_{ac} {}^{(1,1)}\hat{R}_b^d + \frac{1}{2} h_a^d {}^{(1,1)}\hat{R}_{bc} \\
& - h_{ac} \Omega E_b^d + h_{bc} \Omega E_a^d + h_b^d \Omega E_{ac} - h_a^d \Omega E_{bc}
\end{aligned} \tag{14c}$$

$$\mathcal{N}_{\mathbf{E}a} = - {}^{(3)}\nabla_b E_a^b - {}^{(3)}\epsilon_{abc} k^{bd} B_d^c \tag{14d}$$

$$\mathcal{N}_{\mathbf{B}a} = - {}^{(3)}\nabla_b B_a^b + {}^{(3)}\epsilon_{abc} k^{bd} E_d^c \tag{14e}$$

$$\mathcal{N}_{(0,1)\hat{\mathbf{R}}ab} = {}^{(3)}\nabla_a {}^{(0,1)}\hat{R}_b - {}^{(3)}\nabla_b {}^{(0,1)}\hat{R}_a + k_b^c {}^{(1,1)}\hat{R}_{ca} - k_a^c {}^{(1,1)}\hat{R}_{cb} + 2 {}^{(3)}\epsilon_{ab}^c \Omega_d B_c^d \tag{14f}$$

$$\begin{aligned}
\mathcal{N}_{(1,1)\hat{\mathbf{R}}abc} = & {}^{(3)}\nabla_a {}^{(1,1)}\hat{R}_{bc} - {}^{(3)}\nabla_b {}^{(1,1)}\hat{R}_{ac} - \frac{1}{12} h_{ac} {}^{(3)}\nabla_b R + \frac{1}{12} h_{bc} {}^{(3)}\nabla_a R + {}^{(0,1)}\hat{R}_a k_{bc} \\
& - {}^{(0,1)}\hat{R}_b k_{ac} + 2 {}^{(3)}\epsilon_{ab}^d \Omega_0 B_{dc} - 2 \Omega_a E_{bc} + 2 \Omega_b E_{ac} + 2 h_{ca} \Omega_d E_b^d - 2 h_{cb} \Omega_d E_a^d
\end{aligned} \tag{14g}$$

$$\mathcal{N}_{\Omega a} = - {}^{(3)}\nabla_a \Omega + \Omega_a \tag{14h}$$

$$\mathcal{N}_{\Omega_0 a} = - {}^{(3)}\nabla_a \Omega_0 + k_a^b \Omega_b - \frac{1}{2} \Omega {}^{(0,1)}\hat{R}_a \tag{14i}$$

$$\mathcal{N}_{\Omega_a ab} = - {}^{(3)}\nabla_a \Omega_b + h_{ab} \omega + k_{ab} \Omega_0 - \frac{1}{2} \Omega {}^{(1,1)}\hat{R}_{ab} \tag{14j}$$

$$\mathcal{N}_{\omega a} = - {}^{(3)}\nabla_a \omega - \frac{1}{24} \Omega {}^{(3)}\nabla_a R - \frac{1}{12} \Omega_a R + \frac{1}{2} \Omega_0 {}^{(0,1)}\hat{R}_a - \frac{1}{2} \Omega^b {}^{(1,1)}\hat{R}_{ba} \tag{14k}$$

The constraints are, just as the time evolution equations, regular on the whole manifold M including \mathcal{J} . We abstain from proving the propagation of the constraints under the time evolution equations for the first order form of the conformal field equations derived. Since the propagation of the constraints is supported by the following circumstances, there is no serious doubt that they do propagate. First, the propagation has been proven for the forms of the conformal field equations given in [12,10,7]. Second, for the first order form of the Einstein equation derived in [5], which is obtained from the form given by setting $R = 0$, ${}^{(0,1)}\hat{R}_a = 0$, ${}^{(1,1)}\hat{R}_{ab} = 0$, $\Omega = 1$ and hence $d_{abc}^d = \tilde{C}_{abc}^d$, the propagation of the constraints has been proven. And, third, under the numerical time evolution the constraints propagate modulo the order of convergence of the scheme used.

To give initial data we have to find a solution of the constraints. With the exception of cases with high symmetry [3], it is not known yet how to solve the constraints (14) directly for the variables $\underline{f} := (h_{ab}, k_{ab}, \gamma_{bc}^a, E_{ab}, B_{ab}, {}^{(0,1)}\hat{R}_a, {}^{(1,1)}\hat{R}_{ab}, \Omega, \Omega_0, \Omega_a, \omega)$. Nevertheless the existence of solutions of the constraints on $\tilde{\Sigma} \cap \partial\tilde{\Sigma}$ has been proven in [13] for arbitrary topology of $\partial\tilde{\Sigma}$. After solving an elliptic problem for $(h_{ab}, k_{ab}, \Omega, \Omega_0)$, appropriate contractions of (14) can be used to calculate the remaining data. It is shown in [13], that, although divisions by Ω are needed to calculate the curvature related quantities, these curvature quantities are smooth at $\partial\tilde{\Sigma}$, where Ω vanishes ($= \mathcal{S}$), and provide, therefore, suitable data for the time evolution equations. Clearly, this division by Ω is numerically a delicate issue. However, in [14] we will discuss a way of doing this which works for arbitrary \mathcal{S} .

III. THE ROLE OF THE CONFORMAL FACTOR

In the preceeding section we have derived symmetric hyperbolic evolution equations of first order representation from the conformal field equations. Apart from the treatment of

the grid boundaries there are standard techniques available to obtain stable discretisations of symmetric hyperbolic systems. Due to properties distinguishing the conformal approach from approaches working in terms of physical spacetime the treatment of the outer grid boundary can be made trivial, as we will see in the next section. Therefore, it is interesting to understand what kind of physical scenarios can be dealt with by the conformal approach without complicating matters by introducing additional (inner) boundaries.

We will see in this section that the class of scenarios meeting the requirements just mentioned is much larger than the class we would get under these requirements when working in terms of physical spacetime. The underlying reason is the role of the conformal factor Ω . For the equations, and therefore for the discretisations, the conformal factor is just one of many variables which may assume any value. But the conformal factor is a very special variable when transforming back to physical spacetime by rescaling $g_{ab} \mapsto \Omega^{-2}g_{ab}$. Then the $\Omega = 0$ level sets turn out to be boundaries of the physical spacetime. This double role of the conformal factor not only enlarges the class of physical problems which we can treat by standard techniques of numerical mathematics, it also determines the character of the initial value problem we solve.

A. The hyperboloidal initial value problem

Let $\underline{f}(t_0, \vec{x}) = (h_{ab}, k_{ab}, \gamma^a_{bc}, E_{ab}, B_{ab}, {}^{(0,1)}\hat{R}_a, {}^{(1,1)}\hat{R}_a{}^c, \Omega, \Omega_0, \Omega_a, \omega)$ be a smooth solution of the constraints on an everywhere spacelike hypersurface $\bar{\Sigma}_{t_0}$, $\Omega|_{\bar{\Sigma}_{t_0}} \geq 0$, with boundary \mathcal{S}_{t_0} , where Ω vanishes. If $\nabla^a \Omega|_{\mathcal{S}}$ is a future directed, non-vanishing null vector, we call $(\bar{\Sigma}_{t_0}, \underline{f}(t_0, \vec{x}))$ a **hyperboloidal initial value problem**.

We can smoothly extend the hypersurface $\bar{\Sigma}_{t_0}$ and the data $\underline{f}(t_0, \vec{x})$ beyond the boundary to obtain an **extended hyperboloidal initial value problem** $(\Sigma_{t_0}, \underline{f}(t_0, \vec{x}))$. Without loss of generality we assume that $\Omega < 0$ on the extension. For an extended hyperboloidal initial value problem the physical part of the future of Σ_{t_0} is independent of the formal extension of the initial data beyond \mathcal{S} since $\tilde{M} \cap \mathcal{D}(\Sigma) = \mathcal{D}(\tilde{M} \cap \Sigma)$. Therefore, we do not require the extended data to satisfy the constraints outside $\bar{\Sigma}_{t_0}$.

B. Interpretation of various topologies of \mathcal{S}

In this subsection we classify various initial data configurations by finding spacetimes with the same topology of \mathcal{S} . It may well be that the data in each class develop into spacetimes with very different structures in the large. To analyse this variety in detail is an interesting issue and it is a goal of the numerical experiments. Here, our purpose is to only describe a minimal collection of scenarios which we can treat with the conformal approach without introducing inner boundaries.

1. $\tilde{\Sigma}$ s with spherical boundaries

The simplest case of a compact three dimensional manifold $\mathcal{S} \cup \tilde{\Sigma}$ is shown in figure 1, namely the ball B^3 .

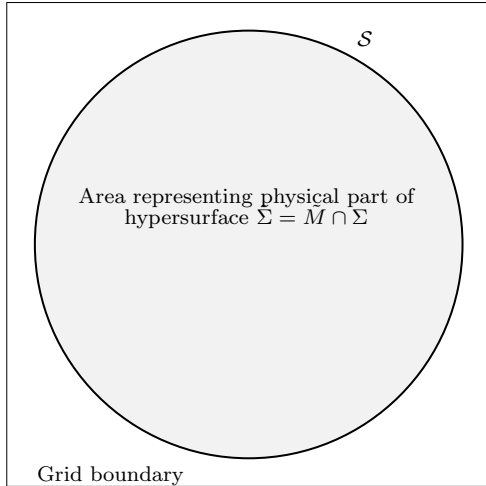


FIG. 1. Data evolving into a space-time with an asymptotic structure as Minkowski spacetime. The third dimension is suppressed, \mathcal{S} is a sphere.

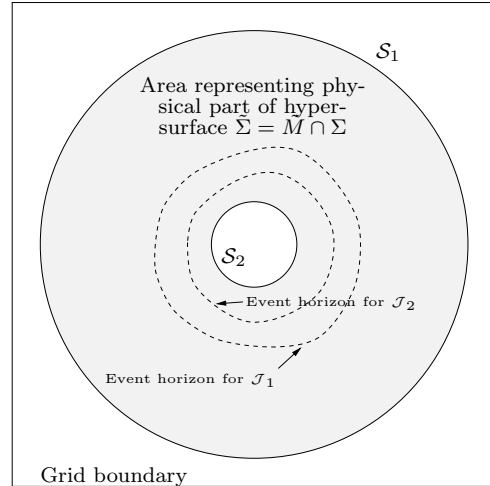


FIG. 2. Data evolving into a space-time with an asymptotic structure as Schwarzschild-Kruskal. The third dimension is suppressed. The \mathcal{S} 's are spheres, the corresponding event horizons are also shown.

Its interior is diffeomorphic to R^3 . For a standard choice of the metric this is a hyperboloidal slice in Minkowski spacetime. For weak data the whole spacetime evolving from the data has an asymptotic structure similar to Minkowski spacetime [6]. Timelike infinity i^+ can be represented by a regular point on the grid. For strong data the spacetime will develop a singularity, there will not be any regular i^+ . In general, we expect strong field configurations to develop regions for which all future directed causal curves end in a singularity and the arising spacetimes will then have at least one event horizon.

The next, slightly more complicated manifold is obtained by cutting out a ball from the interior of the ball as shown in figure 2. The interior $\tilde{\Sigma}$ has topology $R \times S^2$ and there are two \mathcal{S} 's evolving into two \mathcal{J} s. This is the topology of a slice in the conformal picture of the Schwarzschild-Kruskal spacetime (see also figure 5). By Birkhoff's theorem spherically symmetric data with this topology of \mathcal{S} will evolve into the Schwarzschild-Kruskal spacetime with its spacelike singularity in the future. For data close to Schwarzschild data there will probably be a spacelike singularity in the future and there will then be an event horizon around each \mathcal{J} . Therefore it is justified to speak in the situation of figure 2 of a one black hole spacetime, although there may be data for which no singularity appears.

By cutting out N balls from the interior, spacetimes with $N + 1$ \mathcal{J} s are obtained. Figure 3 shows the $N = 2$ case.

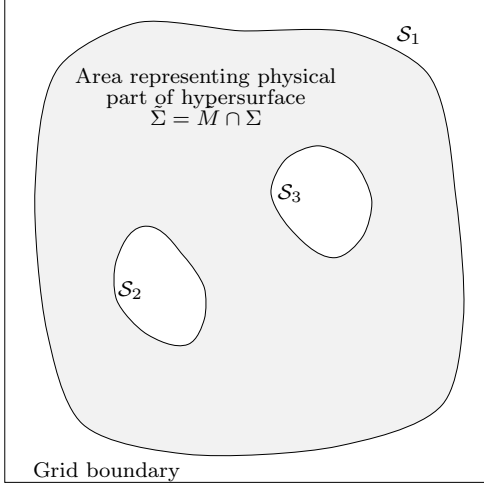


FIG. 3. Data evolving into a space-time with an asymptotic structure as a two black hole spacetime with three disjoint null infinities. The third dimension is again suppressed. The S 's are spheres.

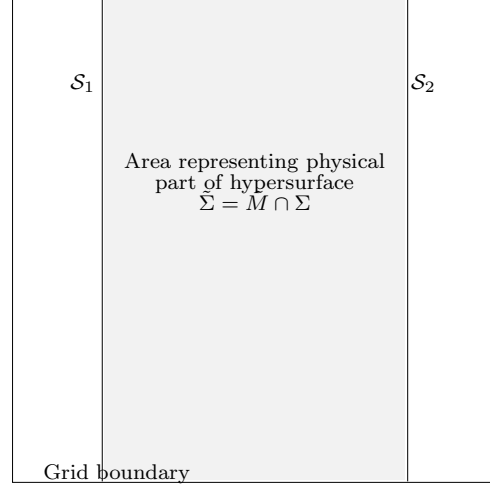


FIG. 4. Data evolving into a space-time with an asymptotic structure as the A3 spacetime. The third dimension is again suppressed. The grid boundaries in the vertical dimension are identified as well as the boundaries in the suppressed dimension. The S 's are tori.

Spacetimes usually interpreted as N black holes with $N+1$ \mathcal{J} 's have hyperboloidal hypersurfaces like the one shown. Whether, in the case $N = 2$ for simplicity, an observer at \mathcal{J}_1 actually sees one or two black holes depends on the slice and the data. If the event horizon of \mathcal{J}_1 consists of two pieces, there are two separated black holes which may merge later, i. e. the two pieces of the event horizon merge.

2. $\tilde{\Sigma}$ s with toroidal and other boundaries

The examples discussed in the preceeding subsection are all asymptotically flat spacetimes which are only a subset of the asymptotically regular spacetimes. Except for one case spacetimes which are asymptotically regular, but not asymptotically flat, will not be discussed here.

Although nowadays computers provide the resources for doing three dimensional calculations with reasonable resolution, high accuracy requirements as needed for certain interesting scenarios may require calculations with higher resolution. Much higher resolutions can be achieved by analysing spacetimes with one Killing vector and they may also be easier to understand as they are easier to imagine and to visualise. In asymptotically flat spacetimes a Killing vector field with closed orbits vanishes at certain points and therefore there is an axis. Coordinate systems adapted to a one Killing vector symmetry become singular at the axis, the evolution equations or the variables are singular there, and numerical instabilities are very difficult to avoid. So it would be very interesting to have spacetimes available which

admit one Killing vector without having an axis, which possess null infinity, and which contain gravitational radiation. Those spacetimes are similar to the Schwarzschild solution, which is a spherically symmetric solution without a centre.

This was the motivation of B. Schmidt to investigate these spacetimes [15]. According to their simplest representative, the A3 solution in the classification of Ehlers and Kundt [16], they are called asymptotically A3. Figure 4 shows the initial slice for an asymptotically A3 spacetime. At the boundary of the suppressed z direction and the vertical y direction points are identified. Both \mathcal{S} 's are tori. The A3 solution has a Killing vector with circular orbits but without axis. Many other asymptotically A3 solutions with two Killing vectors are known [15,17]. In contrast to the spherically symmetric Schwarzschild solution many of them contain gravitational radiation [18].

Asymptotically A3 solutions provide an excellent testbed for numerical codes as they allow us the testing of radiation extraction procedures against exact solutions. They have been intensely used for testing in the conformal codes [11,14]. Details about the tests of the author's code on these examples are going to be reported in [14].

C. \mathcal{J} -fixing

In the hyperboloidal initial value problem the boundaries \mathcal{S} of $\tilde{\Sigma}_{t_0}$ are parts of ingoing null hypersurfaces. For a vanishing shift vector the coordinate area of $\tilde{\Sigma}_t$ shrinks, the physical part of the hypersurface is represented by less and less gridpoints. This loss of resolution is a wide-spread objection against the numerical application of conformal techniques. But this objection is unjustified as the shift vector can always be chosen in such a way that the location of \mathcal{S}_t is fixed and no gridpoints are lost. We call such a choice “ \mathcal{J} -fixing”.

In the spherically symmetric case the author has used such a choice of coordinates in accuracy tests leading to [3]. There were two reasons why this choice was not pursued further: Firstly, the accuracy obtained was lower than the one for the case of an “infalling” \mathcal{J} even for late times and, secondly, i^+ was for that particular choice of coordinates no longer on the grid, the time direction was “decompactified” [unpublished work].

J. Frauendiener has generalised the \mathcal{J} -fixing [11] to the non-spherically symmetric case. In the variables used in this paper the shift vector on \mathcal{J} has to be chosen as follows:

$$N^a|_{\mathcal{J}} = -\frac{N}{\Omega_0} h^{ab} \Omega_b. \quad (15)$$

It is easy to see that (15) plugged into equation (13h) yields $\partial_t \Omega|_{\mathcal{J}} = 0$. The expression is regular on \mathcal{J} as $\nabla_a \Omega$ is a non-vanishing null vector on \mathcal{J} and therefore $\Omega_0 \neq 0$, but Ω_0 may become singular on M/\mathcal{S} . As an alternative everywhere regular on M one can use:

$$N^a = -N \frac{\Omega_0}{(\Omega_0)^2 + (\Omega)^2} h^{ab} \Omega_b. \quad (16)$$

Since N^a depends on variables, equation (13c) contains second derivatives of variables making the system of equations (13) formally “parabolic”. But those derivatives can be eliminated by the use of the other equations yielding a system first order in space and time again. J. Frauendiener has shown that the conformal field equations in spinor formulation

stay symmetric hyperbolic even with \mathcal{J} -fixing [11]. He also demonstrated that \mathcal{J} -fixing works in his two dimensional code.

By using a \mathcal{J} -fixing choice of shift there is no loss in freedom of specifying the shift vector on \tilde{M} , as with a \mathcal{J} -fixing shift N^a the new shift $N^a + \Omega \tilde{N}^a$ is also \mathcal{J} -fixing for arbitrary \tilde{N}^a .

IV. A WAY TO OBTAIN STABLE BOUNDARIES

When solving symmetric hyperbolic equations numerically, the discretisation scheme used must be altered at the boundaries of the grid. It is not only necessary that the treatment must be consistent with the initial boundary value problem of the equations, the interior scheme and the boundary treatment must also fit. Otherwise gridmodes not related to a solution of the continuous equation arise from the boundaries and trigger instabilities. Even for very simple linear equations like the advection equation many discretisations of the boundary are unstable, although they look reasonable.

In general relativity the problem is worse, even the analytic boundary value problem is not completely understood [19]. On a timelike boundary the evolution equations and the constraints must be solved simultaneously. This consistency requirement determines the number of functions which can be specified freely. If the constraints are violated at the boundary, the numbers calculated at the gridpoints influenced by the boundary will not approximate any solution of the Einstein equation. The grid is filled with “invalid points” very quickly, independently of the grid spacing. To make things even worse the error made cannot be estimated by the size of the violation of the constraints [20]. Therefore a discretisation must not only be stable but also consistent with constraint propagation.

Even if one could solve this boundary problem there would still remain the problem of how to suppress artificial backscattering of an outgoing wave when it hits the boundary. Already for the wave equation in two and in three space dimensions that problem is not solvable by a local procedure [21], as the uniquely determined condition for “no backscattering” involves a non-local pseudo-differential operator. Stable local approximations to this non-local pseudo-differential operator show typically an artificial reflection of the order of percent [21].

If it were necessary to calculate a solution of the conformal field equations on the whole grid, the situation would be similarly hopeless. But we do not have to calculate a solution of the conformal field equations on the whole grid. As already pointed out, $\tilde{M} \cap \mathcal{D}(\Sigma) = \mathcal{D}(\tilde{M} \cap \Sigma)$. Therefore one can modify the equations and/or the data outside $\tilde{M} \cup \mathcal{J}$.

The “boundary treatment” we are going to present utilises this property of the conformal field equations and is independent of the exact form of the time evolution equations. To simplify the writing we continue by writing our time evolution equations in the general form

$$\partial_t \underline{f} + \underline{\underline{A}}^i \partial_i \underline{f} - \underline{b} = 0. \quad (17)$$

The $\underline{\underline{A}}^i$ are quadratic matrices depending on \underline{f} , \underline{b} is a vector also depending on \underline{f} .

To obtain equations whose boundary treatment has already been analysed the equations (17) are modified to

$$\partial_t \underline{f} + (1 - \alpha(\Omega)) r^i \partial_i \underline{f} + \alpha(\Omega) (\underline{\underline{A}}^i \partial_i \underline{f} - \underline{b}) = 0, \quad (18)$$

with a sufficiently often differentiable function $\alpha(\Omega)$, which is 0 for $\Omega \leq \Omega_0 < \Omega_1 < 0$ and 1 for $\Omega \geq \Omega_1$. r^i is an outward pointing vector field. For $\Omega_0 > \max_{\text{grid boundary}} \Omega$ one obtains near the boundary an equation with well-analysed boundary discretisations for many interior schemes. For an overview and the proofs of stability see [22,23]. The local order of convergence at the boundary may be one order lower than the convergence order n of the interior scheme without endangering the overall order n [24].

The equations near the boundary are outward directed advection equations. Numerical noise created by a small transition zone $[\Omega_0, \Omega_1]$ is transported to the boundary. Since Ω does not necessarily stay less than Ω_0 , the stability property of the boundary may get lost. By choosing $r^i = 0$ this can be avoided, the time evolution near the boundary gets frozen, one obtains:

$$\partial_t \underline{f} + \alpha(\Omega) (\underline{A}^i \partial_i \underline{f} - \underline{b}) = 0. \quad (19)$$

Of course the possibilities are not restricted to the cases discussed. One could e. g. try to combine the advantages of both methods described by only setting $r^i = 0$ in the equation for Ω .

The change of the system (17) to (18) or (19) will not change the solution on \tilde{M} . Nevertheless the numerically calculated numbers may change on \tilde{M} . In a numerical calculation we have to fulfil the Courant-Friedrich-Levy condition, hence the numerical range of influence of a point is larger than or equal to the analytic range of influence, i. e. values at gridpoints in \tilde{M} may numerically depend on values outside \mathcal{J} . For a convergent scheme the dependence of the calculated solution on the values in the difference Δ of the two ranges must go to zero with the convergence rate. The error made by changing the data or the equations in Δ is of the same size, order, and nature as the discretisation error. This error is automatically taken into account when determining the error bars of the calculated values by a convergence analysis. Therefore, although the numbers actually calculated as an approximation to the solution may be changed by the boundary treatment, the physical predictions made from the numerical experiments do not change, since the physical predictions of a numerical experiment are the numbers modulo the error bars.

Beside the simplification of the boundary treatment the change of the equations outside \tilde{M} has other positive effects. The equation (17) may develop singularities everywhere in the conformal spacetime [3,4]. Since the equations of system (18) or (19) cannot develop singularities for $\Omega < \Omega_0$ the appearance of a singularity outside \tilde{M} becomes less likely.

The treatment of the grid boundaries described above is also independent of the choice of the gauge source functions and the coordinate representation of the light cone which depends on the gauge source functions. For eigenfeld methods, also applicable as boundary treatment [11], this is not the case. The choice of the gauge source functions at the boundary influences the number of outward and inward propagating fields and, therefore, the boundary treatment.

V. ASPECTS OF OUR GEOMETRICAL SETTING

In the preceeding sections we have deduced a set of equations, which is equivalent to the Einstein equation and whose form is adapted to the requirements of numerics. To conclude

this paper, we will now describe on a heuristic level, based on the rigorous statements of the preceeding sections, how we proceed to calculate a spacetime from the initial slice. We do this on two examples of general interest and compare on those with alternative approaches.

In the first example we illustrate by means of a Penrose diagram what part of a spacetime we can in principle calculate. To use a sufficiently rich example, i. e. an example for which inner and outer boundaries were believed to be needed, but still a simple enough to possess a depictable Penrose diagram, we have chosen the Schwarzschild-Kruskal spacetime. In the second example we explain on the scenario of an energy/matter concentration collapsing to a black hole how gravitational radiation propagates through the conformal spacetime.

A. Evolving spacetime from an initial slice

In figure 5 the Penrose diagram of the Schwarzschild-Kruskal spacetime is shown.

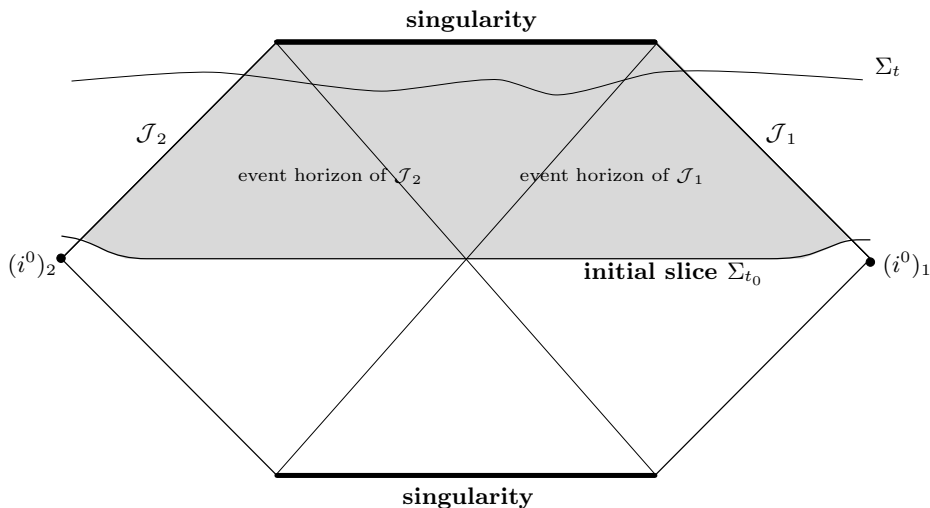


FIG. 5. Penrose diagram of the Schwarzschild-Kruskal spacetime showing the region which can be calculated in the conformal approach. All points with the exception of the two spacelike infinities $(i^0)_1$ and $(i^0)_2$ represent an S^2 .

In the numerical construction of this spacetime from an extended hyperboloidal initial value problem we give appropriate data on an extended hyperboloidal slice Σ_{t_0} . The grid boundaries are placed outside the region representing the physical part of the initial slice. By solving the conformal field equations we calculate a slicing Σ_t of the future of Σ_{t_0} . In principle there is no reason, assuming appropriate coordinates, which prevents us from calculating the whole domain of dependence of the physical part $\tilde{\Sigma}_{t_0}$ of Σ_{t_0} up to the singularity, i. e. to calculate the solution of the Einstein equation in the shaded region of the figure. The conformal field equations can be viewed as the Einstein equation for an artificial spacetime with an artificial matter field, namely the rescaling factor. With this analogy in mind it becomes obvious that the relation between coordinate choice and exhaustive slicing of the spacetime is similar in conformal and physical spacetime.

We now describe how the same situation is approached in two alternative numerical approaches, namely the approach of solving the initial boundary value problem in physical

spacetime and the so-called Cauchy characteristic matching approach.

Figure 6 shows the Penrose diagram of the first case, the approach by solving the initial boundary value problem in physical spacetime as described in [25].

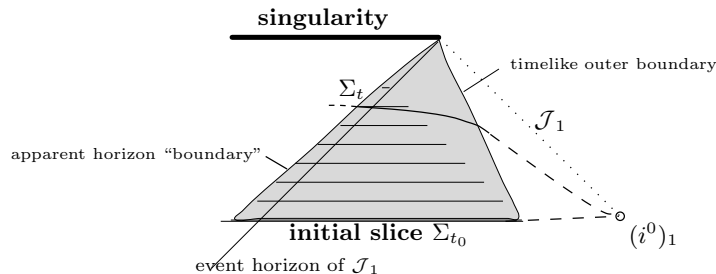


FIG. 6. The part of the Penrose diagram of Schwarzschild spacetime which is calculated when solving the initial boundary value problem in physical spacetime. Again every point represents an S^2 .

Data are given on a compact part of a spacelike initial slice, which is covered by grid-points, and on the boundaries. To be representative for the whole slice, which has topology $R \times S^2$, the compact part should have topology $I \times S^2$, where I is a closed interval. The inner edge of that closed interval I is placed somewhere inside the event horizon, since then its treatment will not influence the physical predictions. For technical reasons the inner “boundary” is often placed near the apparent horizon and therefore called apparent horizon boundary, although the apparent horizon is a null or spacelike hypersurface. In contrast to the inner edge the outer edge of the grid is treated in such a way that it forms a timelike boundary under time evolution. Due to the problem of not having a consistent outer boundary treatment without artificial back scattering, the numerical solution will be consistent with the Einstein equation in the hatched triangle only. The actual size of the hatched region depends on how much gridpoints one can afford to provide to cover the parts of the hypersurface far away. Assuming a consistent outer boundary treatment one would get the shaded region. Null infinity can never be covered, even after rescaling, for the spacelike surfaces used go to spacelike infinity as sketched by the dashed lines.

The approximate radiation extraction methods suggested require being “far away” to give a reasonable approximation for the actually emitted radiation. Nevertheless reading off radiation at a finite distance causes an approximation error. Hence the error made will not converge to zero when refining the grid. It has therefore been suggested to combine the grid refinements with placing the outer boundary further out. There are two problems with this “solution”. Firstly, the number of required gridpoints grows much faster than in the case of only refining and this additional growth certainly outweighs the benefits from computational science efforts to optimise memory footprint and execution speed per gridpoint. Secondly, whenever we place the boundary at a different distance we solve a different problem. This change of the problem does not occur in the conformal method, since the grid contains for every refinement level the conformally completed spacetime and null infinity.

The second alternative we compare with, Cauchy characteristic matching [26], is shown in figure 7.

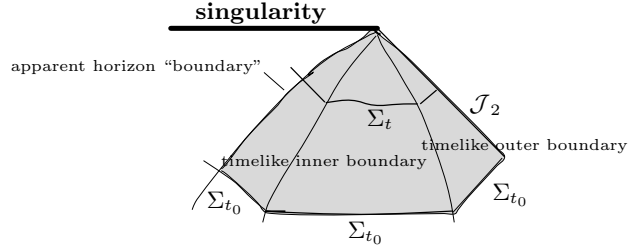


FIG. 7. The part of the Penrose diagram of Schwarzschild spacetimes which is calculated in the Cauchy characteristic approach. Again every point represents an S^2 .

Near the outer edge and near the apparent horizons the spacetime is sliced by null hypersurfaces. The inner null hypersurfaces are cut off inside the apparent horizon. The region between the null hypersurfaces is evolved via a Cauchy problem. As null hypersurfaces unavoidably develop caustics for strong data, the Cauchy slicing in the middle is necessary and must stretch out sufficiently far. Matching the two schemes introduces artificial boundaries and causes stability problems [26]. Although null infinity is mapped to gridpoints by a coordinate rescaling, null infinity remains a true numerical boundary as the equations used are singular there.

As a conclusion we find that in all approaches only part of the whole spacetime can be calculated. But this does not favour the other approaches discussed, because none of them allows us to calculate a larger part of the Penrose diagram. Even when using the data on Σ_{t_0} to integrate backwards in time, as done in [27][figure Va], the neighbourhood of the i^0 s cannot be obtained. To obtain the whole Penrose diagram one would have to start with an initial slice containing spacelike infinity. The conformal metric at i^0 is in general not sufficiently smooth, some of the variables used in the conformal field equations are not well-behaved at i^0 . Therefore the more advanced and complicated conformal techniques of [28] would be required.

B. “Tracking radiation sufficiently far” or “The need for apparent horizons”

Probably the simplest scenario which involves gravitational radiation and for which apparent horizon boundary conditions have been regarded as necessary is an energy/matter concentration collapsing to a black hole.

Figure 8 shows in a diagram how this scenario is calculated in the conformal approach. Its correctness has been justified by the model calculations discussed in [3,4].

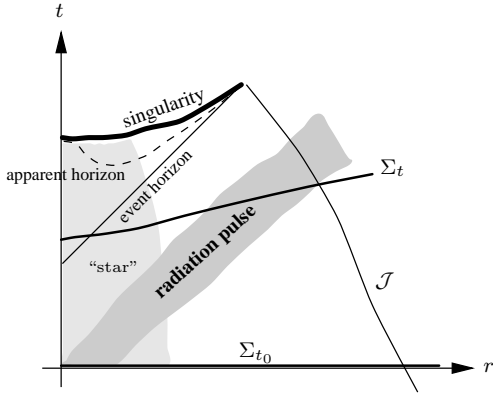


FIG. 8. Cauchy slices in conformal spacetime (= hyperboloidal slices in physical spacetime)

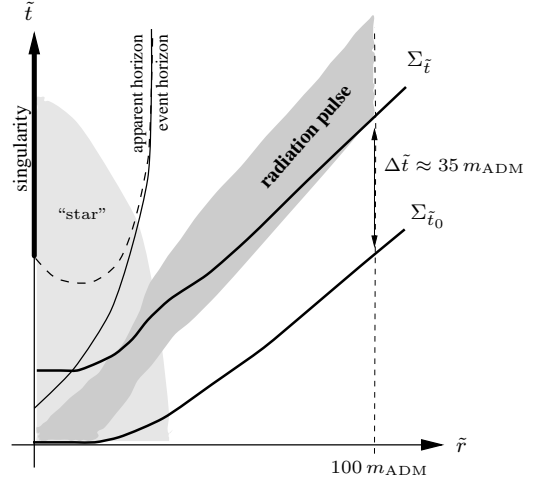


FIG. 9. Hyperboloidal slices in physical spacetime

In the situation drawn a singularity avoiding slicing of the conformal spacetime is in no way pathologic — null infinity, timelike infinity, and the singularity are all at finite conformal coordinate time. A pulse of radiation will propagate outward with a slope of order one and will cross \mathcal{J} at finite conformal coordinate time. When this pulse crosses \mathcal{J} we can read off the radiation which is seen by an observer at infinite physical distance. Although the physical distance between the gridpoints becomes very large near \mathcal{J} , the number of gridpoints used for resolving a signal, as indicated by the width of the pulse, stays approximately constant. The mathematical reason behind this feature is the invariance of the light cone under conformal rescalings.

If we translate figure 8 to physical spacetime coordinatized by physical time \tilde{t} and by physical distance \tilde{r} we get figure 9. The hyperboloidal character of the hypersurfaces Σ_t becomes obvious, for large distances the hypersurfaces approach null hypersurfaces. Since the hypersurfaces are almost null far out, the finite, but far distance at which we want to read off radiation does not significantly influence the integration time required. In the example shown we would need to calculate a numerical time evolution for $\tilde{t} = 35 m_{\text{ADM}}$ to be able to read off radiation at $\tilde{r} = 100 m_{\text{ADM}}$.

We also see that these “physical” coordinates do not very well represent the causal structure of the spacetime near and inside the event horizon — the singularity and the event horizon look like timelike lines. Furthermore we notice that in the interior the slices cease to be regular after a finite time, whereas in the exterior they exist forever. Therefore, if we would like to calculate the longtime behaviour as seen by an observer outside the event horizon we must either distort the hypersurface somewhere or cut out the interior part.

Figure 10 shows the situation in the physical spacetime with singularity avoiding slices, the slicing which is believed to be the most appropriate way for approaching the problem in physical spacetime.

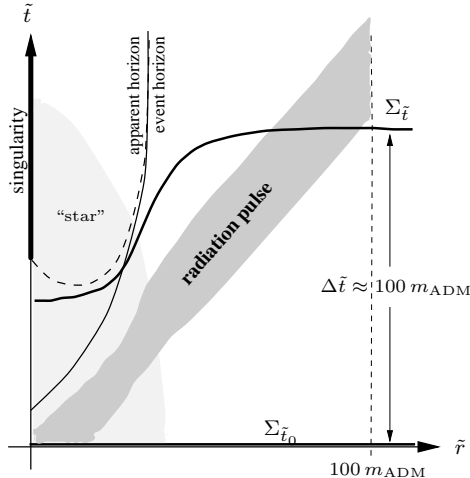


FIG. 10. Cauchy slices in physical spacetime

It is obvious that if we want to read off radiation at $\tilde{r} = 100 m_{\text{ADM}}$, we need to calculate the time evolution up to $\tilde{t} = 100 m_{\text{ADM}}$, and if we want to read it off at $\tilde{r} = 1000 m_{\text{ADM}}$, we even need to integrate to $\tilde{t} = 1000 m_{\text{ADM}}$. Therefore, even if we are only interested in gravitational radiation but not in the longtime behaviour of the spacetime, it is necessary to numerically integrate for a long time, at least in the exterior. To not hit the singularity when doing so one again either has to deal with a significant distortion of the hypersurfaces, i. e. large gradients of the variables somewhere on the hypersurfaces, or one has to cut out the interior of the hypersurfaces, which is the purpose of using apparent horizon boundary conditions.

From what has been said about figure 9 and 10 one might be tempted to utilize hyperboloidal slices in the physical spacetime for the numerical calculation. This would, unfortunately, introduce new problems. They would arise from the fact that the evolution equations require spacelike surfaces but the hyperboloidal slices are almost null in the far zone. Technically, the lapse and/or shift degenerate when a hypersurface becomes almost null. Since in conformal spacetime the hyperboloidal hypersurface is a normal Cauchy surface even at null infinity and beyond, this problem does not arise in the conformal approach.

VI. CONCLUSION

Starting from the conformal field equations we have derived a symmetric hyperbolic first order system determining the time evolution. The system obtained is in a form which allows us to apply standard techniques to discretise in the interior as well as on the grid boundaries. The stability of the resulting schemes is then guaranteed by theorems in the literature. We have seen that an application of only these techniques allows us in principle to calculate the complete future of the initial data for many interesting scenarios, e. g. N black holes.

ACKNOWLEDGEMENT

I would like to thank all the visitors and members of the Albert Einstein institute who were available for numerous discussions concerning the conformal field equations and their numerical implementation.

In particular I would like to mention H. Friedrich, B. Schmidt, and J. Frauendiener for many fruitful discussions.

- [1] H. Friedrich, Proc. R. Soc. London **A 375**, 169 (1981).
- [2] H. Friedrich, Proc. Roy. Soc. **A 378**, 401 (1981).
- [3] P. Hübner, Ph.D. thesis, Ludwig-Maximilians-Universität München, 1993.
- [4] P. Hübner, Phys. Rev. D **53**, 701 (1996).
- [5] H. Friedrich, Class. Quantum Grav. **13**, 1451 (1996).
- [6] H. Friedrich, J. Differential Geometry **34**, 275 (1991).
- [7] J. Frauendiener, gr-qc **9712**, 1 (1997).
- [8] R. Penrose, in *Battelle Rencontres* (Benjamin, New York, 1967), pp. 121–235.
- [9] H. Friedrich, Commun. Math. Phys. **91**, 445 (1983).
- [10] P. Hübner, Class. Quant. Grav. **12**, 791 (1995).
- [11] J. Frauendiener, gr-qc **9712**, 1 (1997).
- [12] H. Friedrich, Commun. Math. Phys. **100**, 445 (1985).
- [13] L. Andersson, P. T. Chruściel, and H. Friedrich, Comm. Math. Phys. **149**, 587 (1992).
- [14] P. Hübner, In preparation.
- [15] B. G. Schmidt, Class. Quant. Grav. **13**, 2811 (1996).
- [16] J. Ehlers and W. Kundt, in *Exact Solutions of the Gravitational Field Equations*, edited by L. Witten (J. Wiley & Sons, New York, 1962), Chap. 2, pp. 49–101.
- [17] P. Hübner, Class. Quantum Grav. **15**, L21 (1998).
- [18] T. Foertsch, Master’s thesis, Techn. Universität Berlin, 1997.
- [19] H. Friedrich and G. Nagy, Commun. Math. Phys. (1999), in print.
- [20] M. W. Choptuik, Phys. Rev. D **44**, 3124 (1991).
- [21] B. Engquist and A. Majda, Mathematics of Computation **31**, 629 (1977).
- [22] S. Abarbanel and D. Gottlieb, Mathematics of Computation **33**, 1145 (1979).
- [23] S. S. Abarbanel and E. M. Murman, in *Proc. Symp. Numerical Boundary Condition Procedures* (NASA, Springfield, 1981), pp. 199–207.
- [24] B. Gustafsson, Mathematics of Computation **29**, 396 (1975).
- [25] P. Anninos *et al.*, Phys. Rev. D **52**, 2059 (1995).
- [26] R. Gómez *et al.*, gr-qc **9801**, 1 (1998).
- [27] P. Hübner, *Numerical Relativity Conference* (Penn State University, State College, 1993).
- [28] H. Friedrich, Journal of Geometry and Physics **24**, 83 (1998).